Electronic Supplementary Material (ESI) for Journal of Materials Chemistry A.


# Supplementary Information

## Metal-Organic Framework based Foams for Efficient Microplastic Removal

Yong-Jun Chen,[a] Yifa Chen,*[ab] Chang Miao,[a] Yi-Rong Wang,[a] Guang-Kuo Gao,[a] Ru-Xin Yang,[a] Hong-Jing Zhu,[a] Jian-Hui Wang,[a] Shun-Li Li[a] and Ya-Qian Lan*[a]

a. *Jiangsu Collaborative Innovation Centre of Biomedical Functional Materials, Jiangsu Key Laboratory of New Power Batteries, School of Chemistry and Materials Science, Nanjing Normal University, Nanjing 210023, P. R. China.*

b. *Changzhou Institute of Innovation & Development, Nanjing Normal University, Nanjing 210023, P. R. China.*

**Corresponding authors Y. C. E-mail: chyf927821@163.com; Y.-Q. L. E-mail: yqlan@njnu.edu.cn*

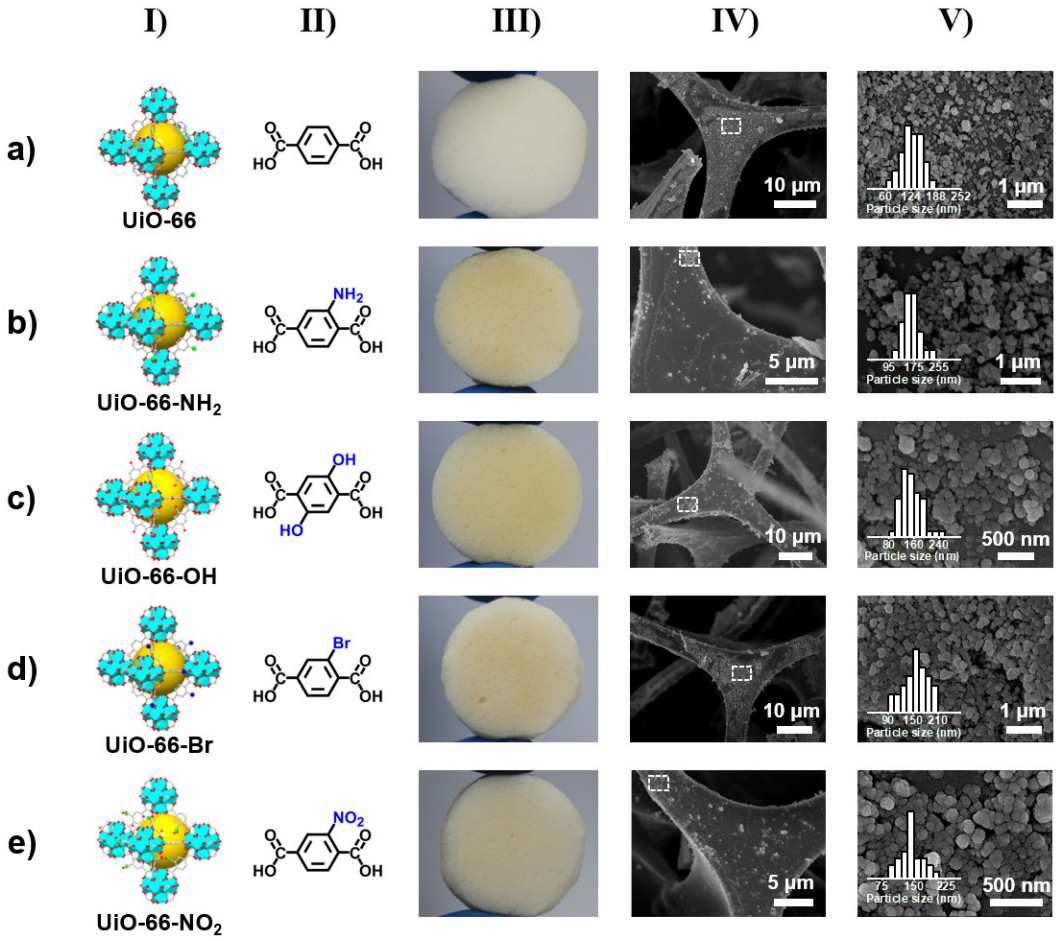


**Fig. S1** The structures and morphologies characterization of the MOF-based foams (UiO-66-X@MF, X = H, $NH_2$, OH, Br and $NO_2$). a) UiO-66@MF. b) UiO-66-$NH_2$@MF. c) UiO-66-OH@MF. d) UiO-66-Br@MF. e) UiO-66-$NO_2$@MF. I) The structure images of UiO-66-X (X = H, $NH_2$, OH, Br and $NO_2$). II) The ligands of UiO-66-X. III) The photo images of UiO-66-X@MF. IV, V) The SEM images of UiO-66-X@MF (insert is the particle size distribution calculated based on more than 200 particles).

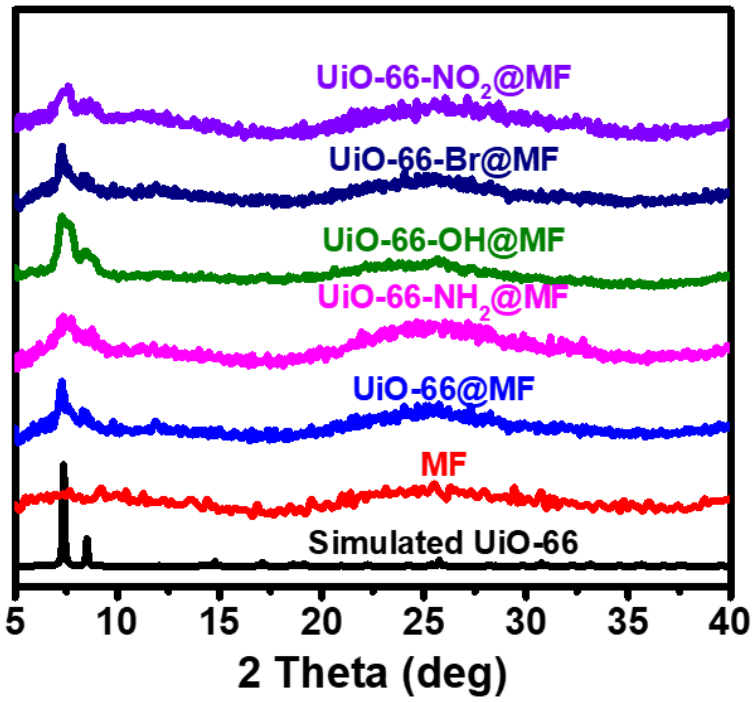


**Fig. S2** The PXRD patterns of bare MF and UiO-66-X@MF (X = H, $NH_2$, OH, Br and $NO_2$).

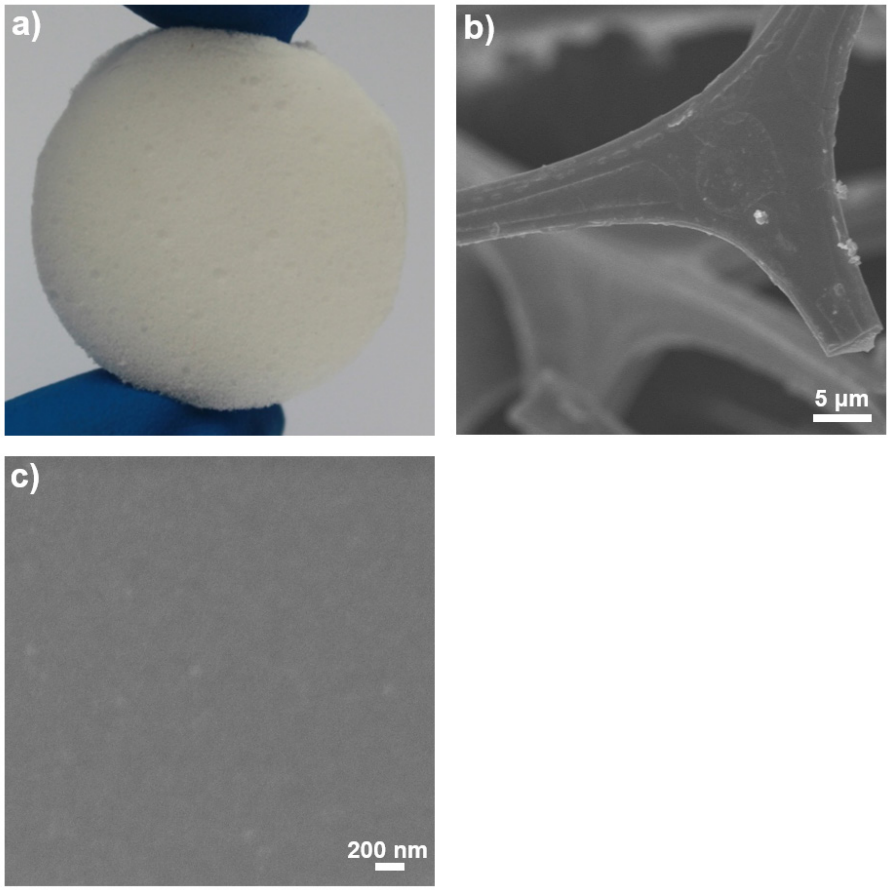


**Fig. S3** The photo and SEM images of bare MF. a) The photo image. b, c) The SEM images.

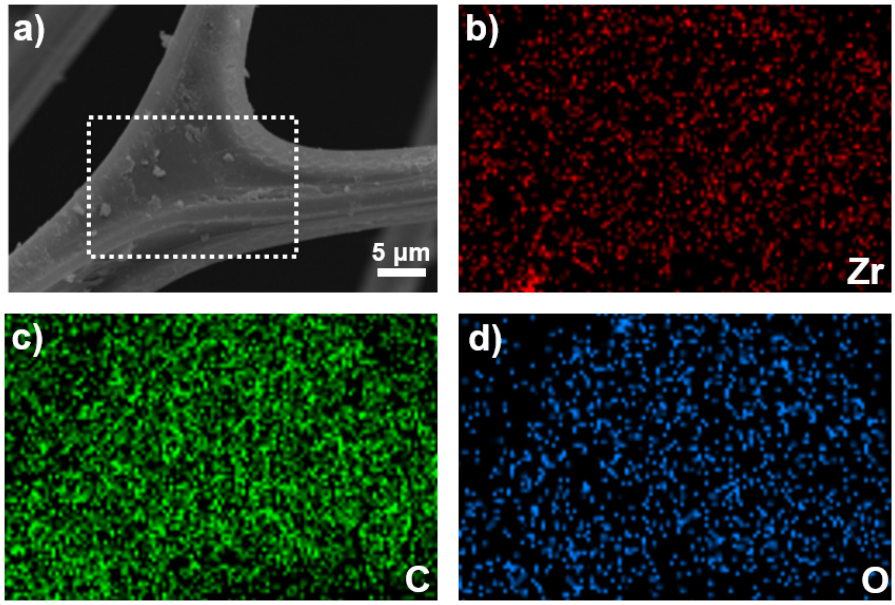


**Fig. S4** The elemental mapping analysis of UiO-66-OH@MF-3. a) The SEM image of UiO-66-OH@MF-3. b) Zr. c) C. d) O.

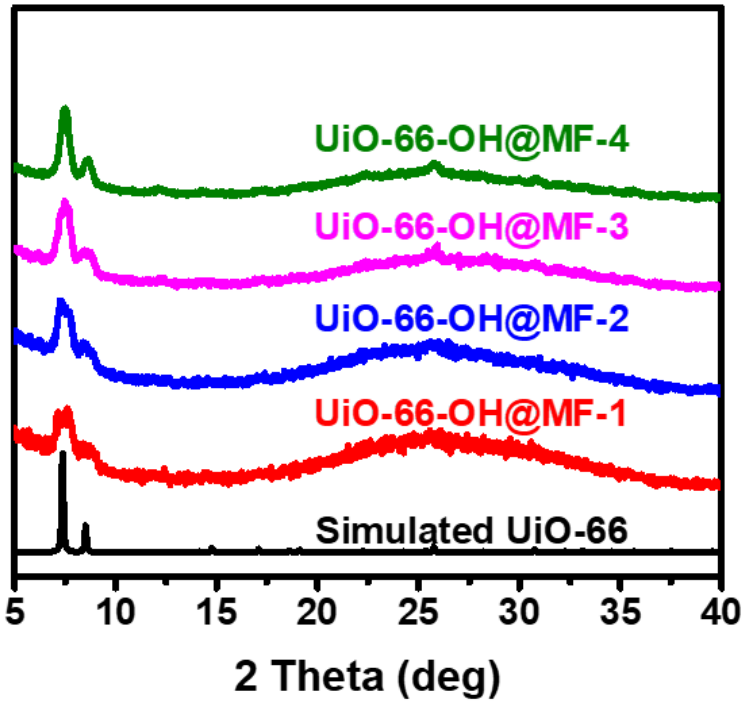


**Fig. S5** The PXRD patterns of UiO-66-OH@MF with different loadings.

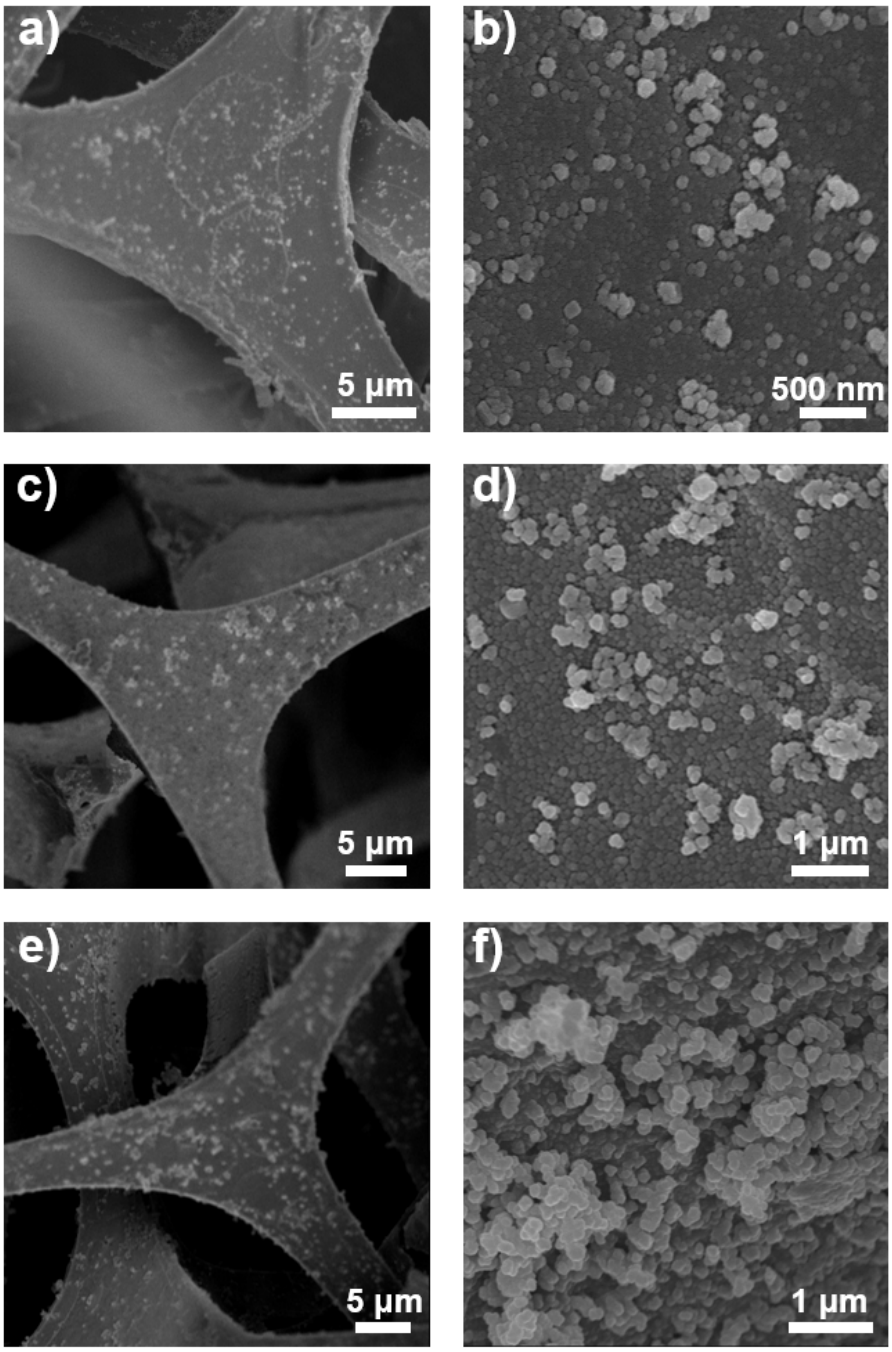


**Fig. S6** The SEM images of UiO-66-OH@MF with different loadings. a, b) UiO-66-OH@MF-1. c, d) UiO-66-OH@MF-2. e, f) UiO-66-OH@MF-4.

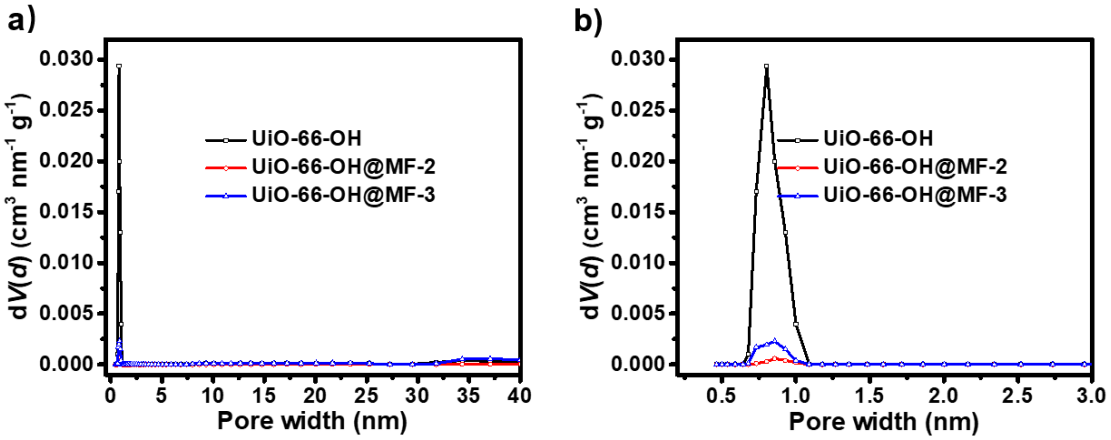


**Fig. S7** The pore size distribution of UiO-66-OH and UiO-66-OH@MF-n (n = 2 and 3). a) 0-40 nm. b) 0-3 nm.

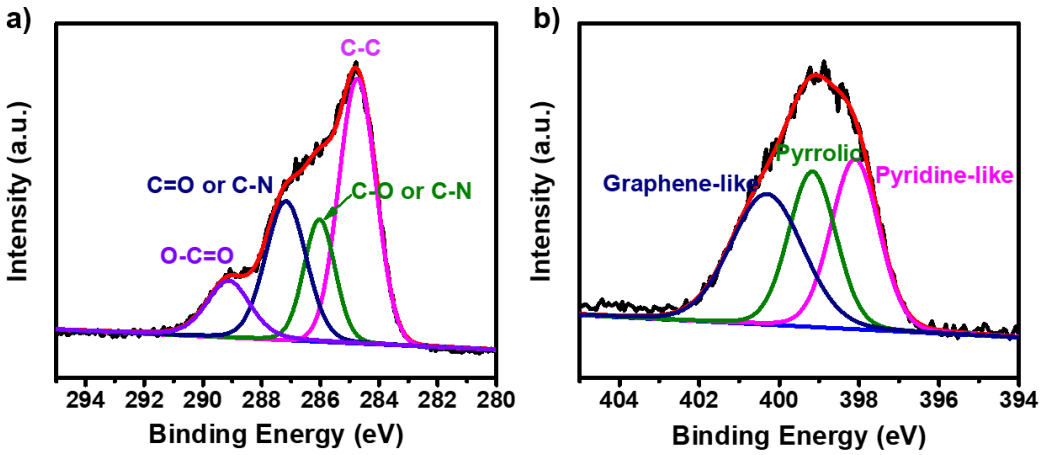


**Fig. S8** XPS spectra of bare MF. a) C1s. b) N1s.

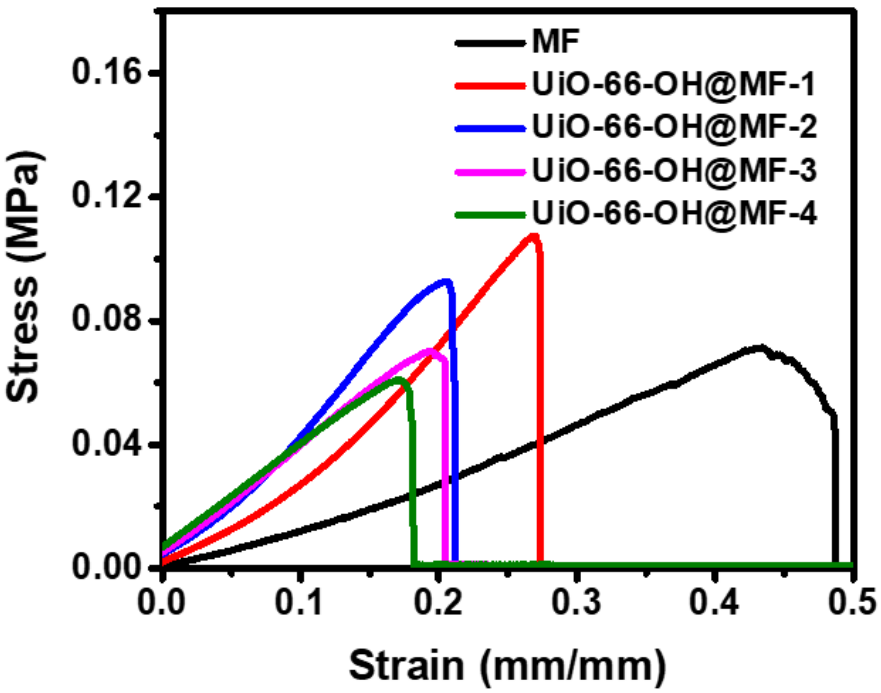


**Fig. S9** The stretching tests of UiO-66-OH@MF with different loadings.

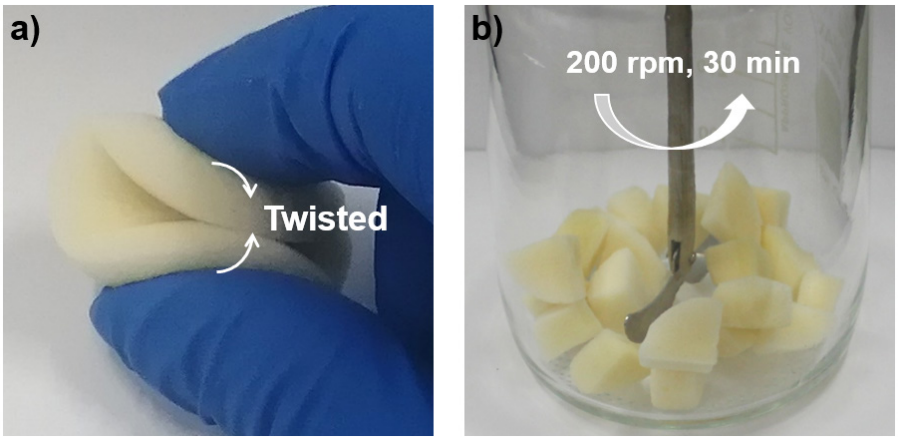


**Fig. S10** Photo images of the twisted and mechanical stirring test for UiO-66-OH@MF-3. a) Twisting test. b) Mechanical stirring test.

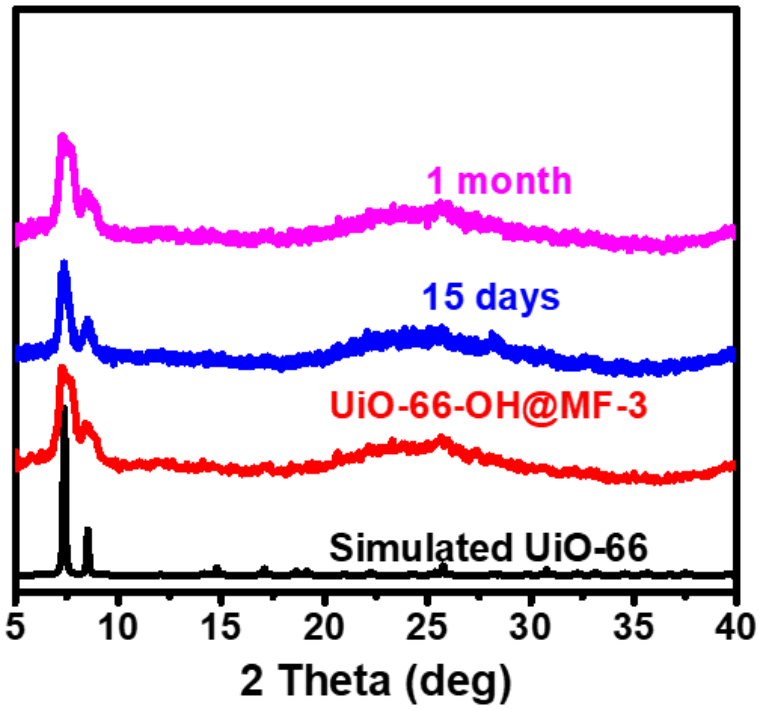


**Fig. S11** The PXRD patterns of UiO-66-OH@MF-3 during water stability tests.

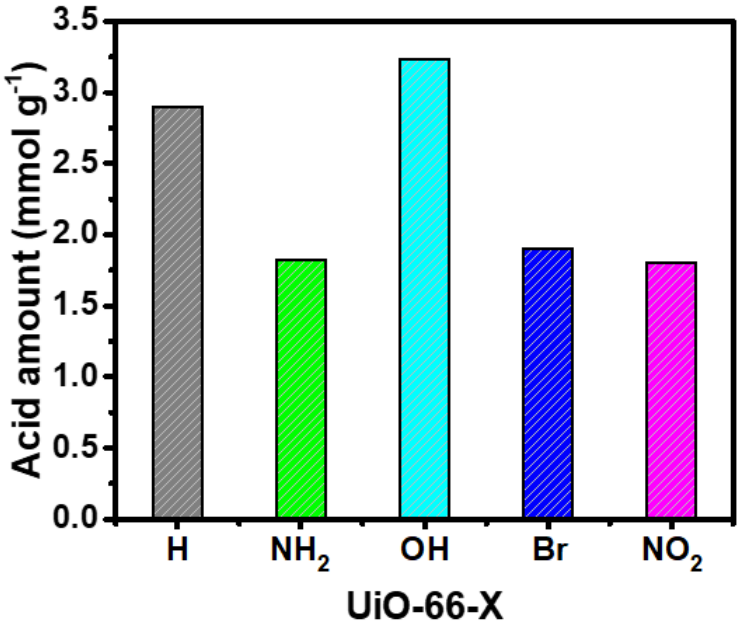


**Fig. S12** The acid amount of UiO-66-X (the selected temperature range is 50-350 $^{o}$C). The $NH_3$-TPD tests is conducted by the pulse technique using a Micromeritics Auto Chem II 2920 instrument using TCD detection. Before $NH_3$-TPD tests, the sample was outgassed at 150 $^{o}$C for 24 h. During the $NH_3$-TPD tests, a sample of 100 mg is pretreated under a flow of helium (30 mL min$^{-1}$) at 180 $^{o}$C for 2 h to remove water. Then the temperature is lowered to RT under a flow of He. The ammonia adsorption is performed at 100 $^{o}$C for about 20 min. The $NH_3$-TPD datas are collected from 50 $^{o}$C to 350 $^{o}$C at a heating rate of 10 $^{o}$C min$^{-1}$ in a helium flow. The amount of physically adsorbed ammonia is collected to further reflect the acidity amount and defects of UiO-66-X (X = H, $NH_2$, OH, Br and $NO_2$).

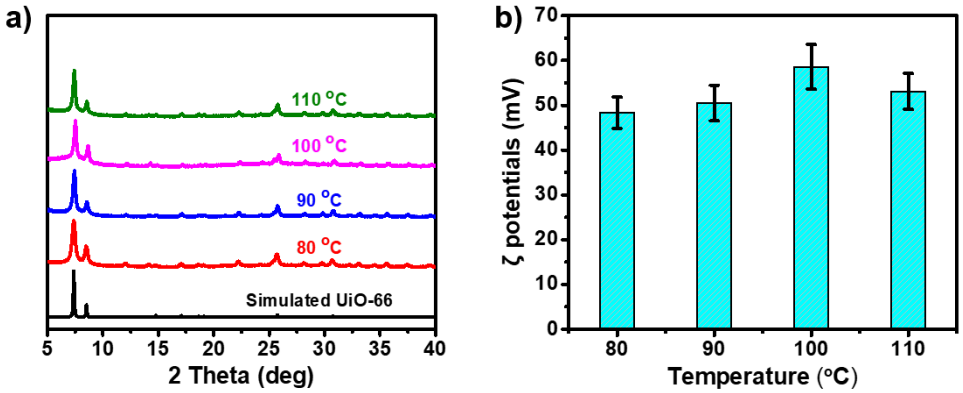


**Fig. S13** The PXRD patterns and ζ potentials of UiO-66-OH obtained from different synthetic temperatures (80, 90, 100 and 110 $^{o}$C). a) PXRD patterns. b) ζ potentials.

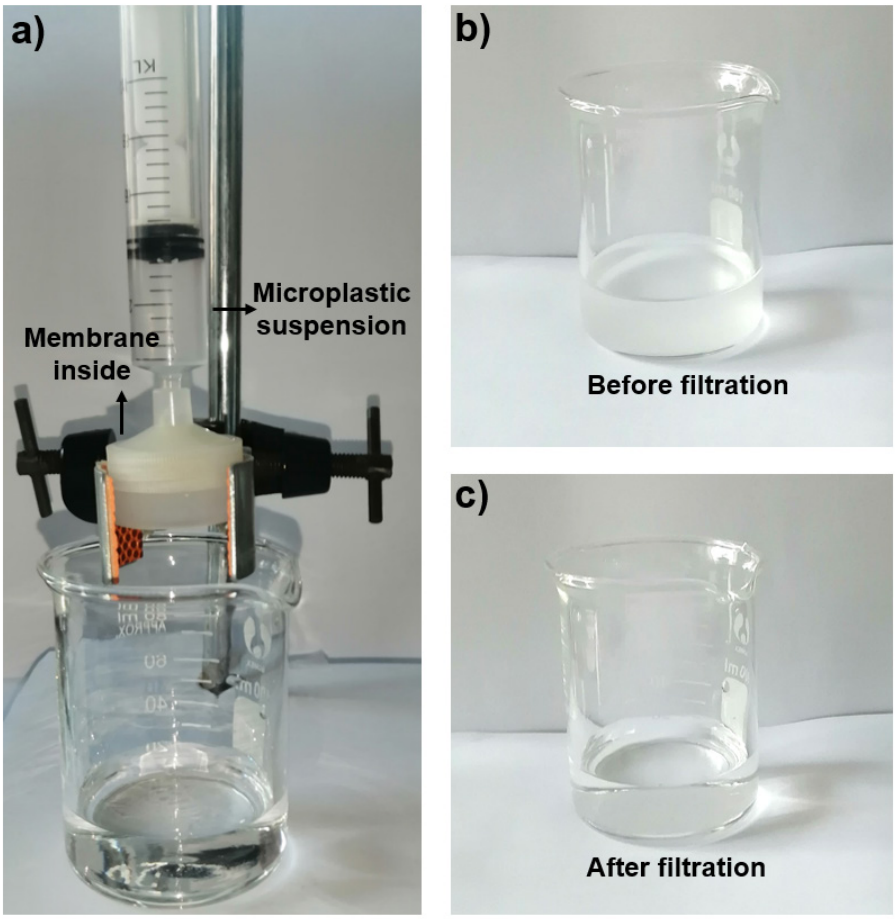


**Fig. S14** The filtration device for the microplastic removal tests. a) Filtration device (flow rate: ~1.2 L $h^{-1}$). b) Simulated microplastic suspension before filtration. c) Simulated microplastic suspension after filtration.

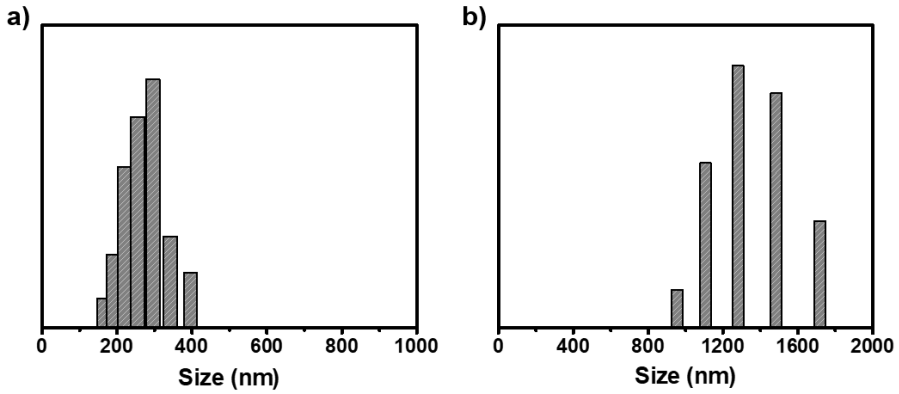


**Fig. S15** The dynamic light scattering (DLS) tests for PVDF (Mw. $5.34 \times 10^5$ g $mol^{-1}$) nanoparticles in different solvents. a) Simulated microplastic solution ($V_{water}$ : $V_{ethanol}$ = 3 : 1) (~273 nm). b) PVDF in water (~1352 nm).

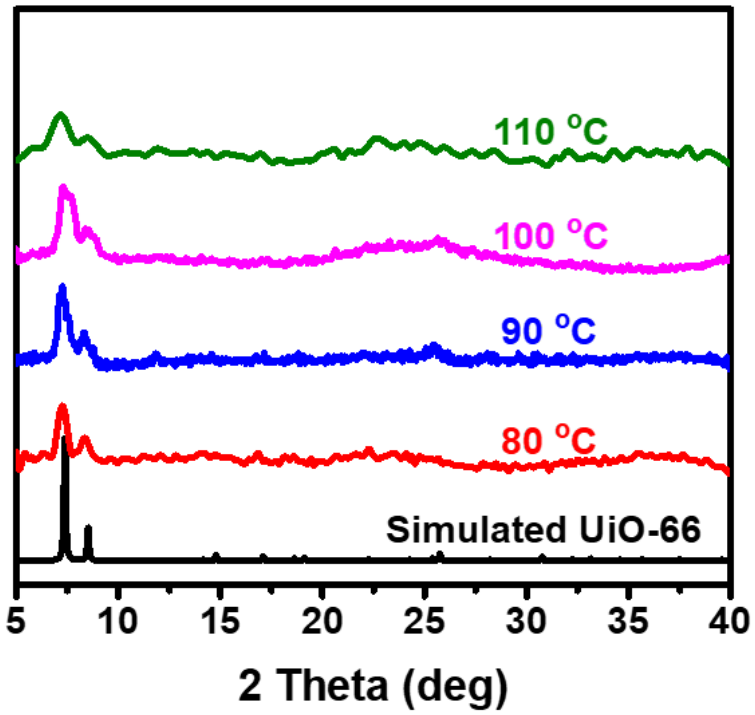


**Fig. S16** The PXRD patterns of UiO-66-OH@MF-3 obtained from different temperatures (80, 90, 100 and 110 °C).

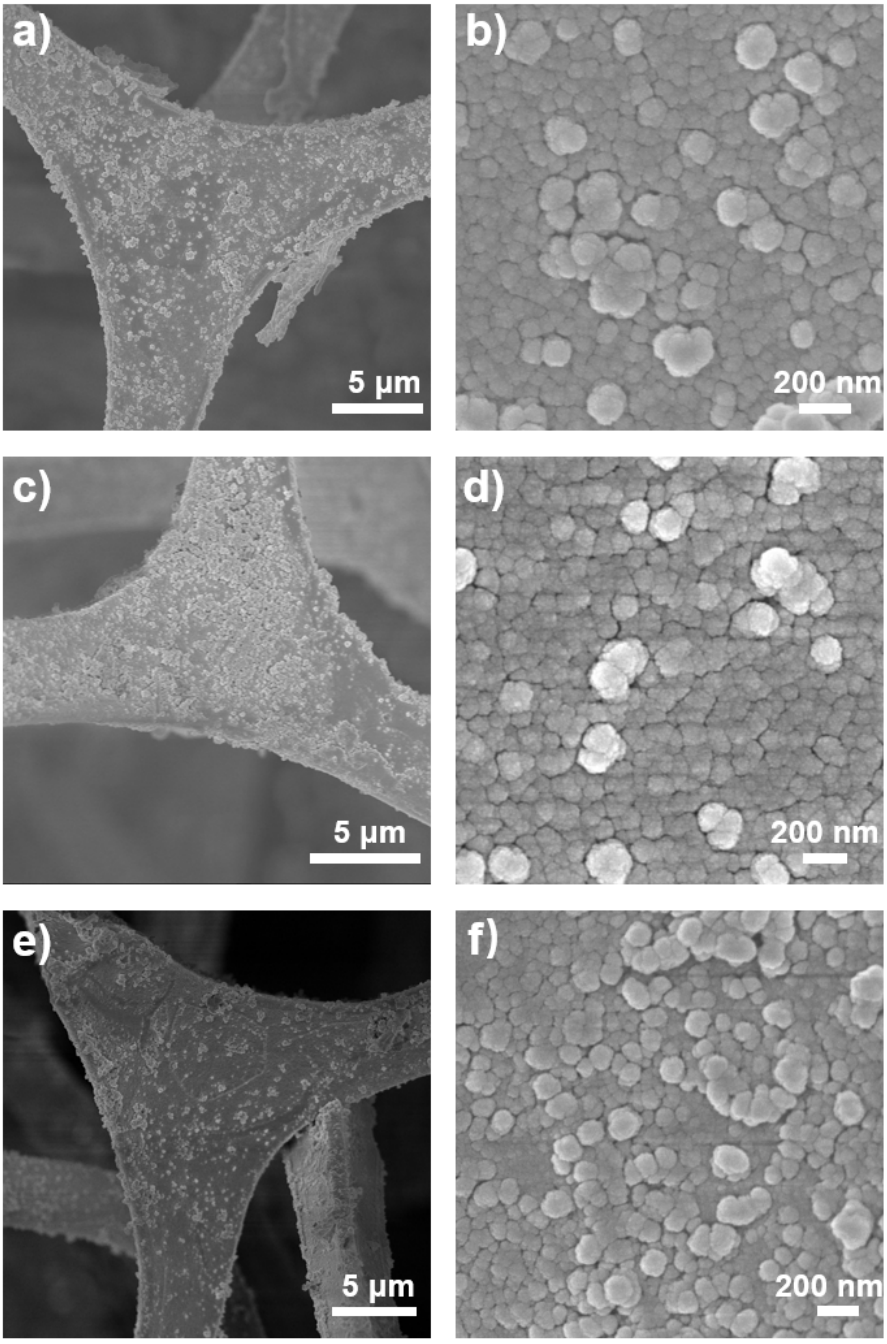


**Fig. S17** The SEM images of UiO-66-OH@MF-3 obtained from different synthetic temperatures. a, b**)** 80 $^{o}$C. c, d) 90 $^{o}$C. e, f) 110 $^{o}$C.

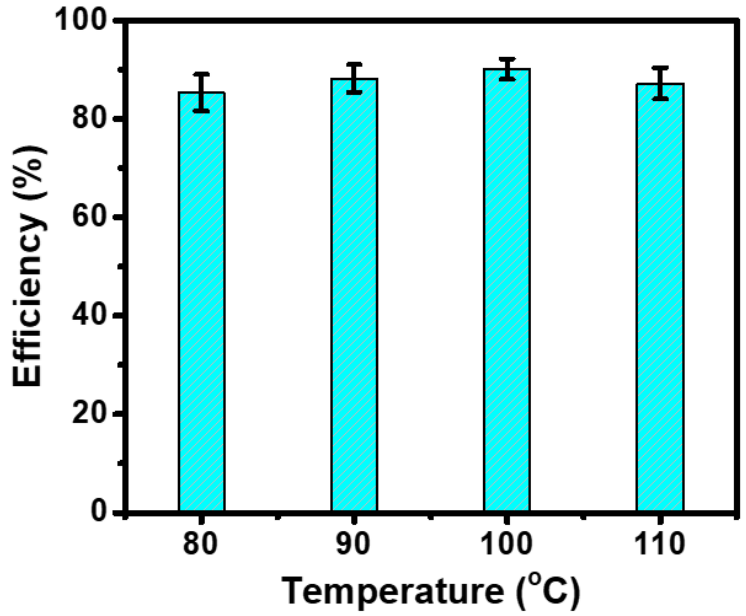


**Fig. S18** The removal efficiency of UiO-66-OH@MF-3 with different synthetic temperatures (80, 90, 100 and 110 $^{o}$C).

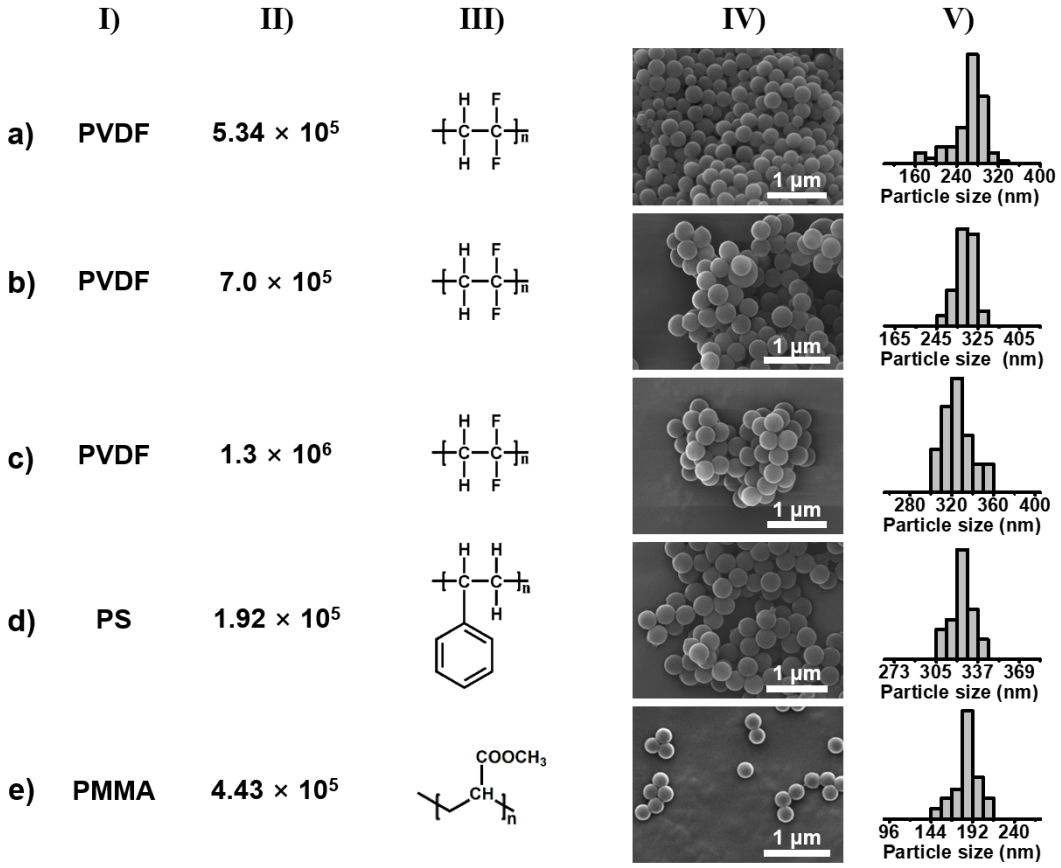


**Fig. S19** The SEM images and particle size of different microplastics. a) PVDF (Mw. 5.34 × $10^5$ g $mol^{-1}$). b) PVDF (Mw. 7.0 × $10^5$ g $mol^{-1}$). c) PVDF (Mw. 1.3 × $10^6$ g $mol^{-1}$). d) PS (Mw. 1.92 × $10^5$ g $mol^{-1}$). e) PMMA (Mw. 4.43 × $10^5$ g $mol^{-1}$). I) Different types of microplastics. II) $M_w$ (g $mol^{-1}$). III) Molecular formula. IV) SEM images. V) particle sizes of different microplastics (PVDF, 5.34 × $10^5$ g $mol^{-1}$, ~260 nm; PVDF, 7.0 × $10^5$ g $mol^{-1}$, ~300 nm; PVDF, 1.3 × $10^6$ g $mol^{-1}$, ~322 nm; PS, 1.92 × $10^5$ g $mol^{-1}$, ~183 nm and PMMA, 4.43 × $10^5$ g $mol^{-1}$, ~325 nm).

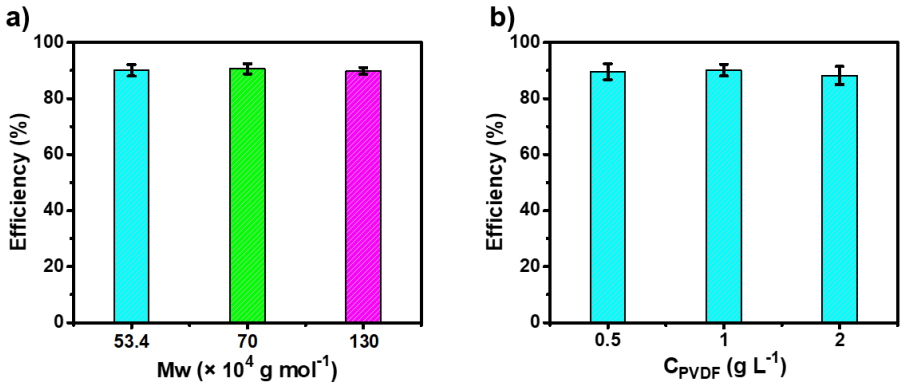


**Fig. S20** The removal efficiency of UiO-66-OH@MF-3 for PVDF based simulated microplastic suspension with different PVDF types and concentrations. a) PVDF based simulated microplastic suspensions with different PVDF types. b) PVDF (Mw. 5.34 × $10^5$ g $mol^{-1}$) based simulated microplastic suspensions with different concentrations.

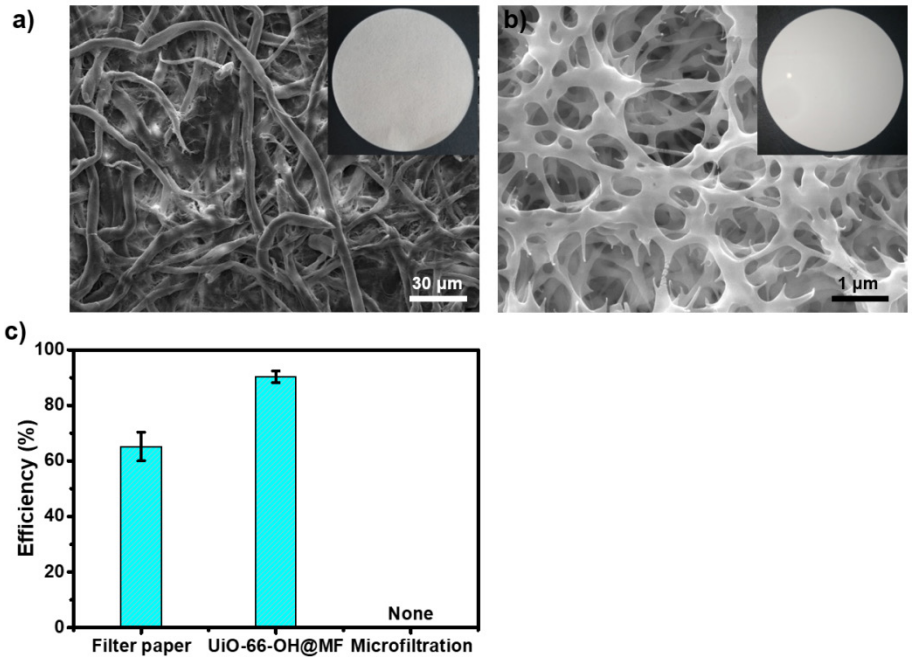


**Fig. S21** The SEM images and removal efficiency of comparative materials (filter paper (20-25 μm) and microfiltration membrane (0.22 μm)). a) The SEM and photo images of filter paper. b) The SEM and photo images of microfiltration membrane. c) The removal efficiency for filter paper, UiO-66-OH@MF and microfiltration membrane in the filtration of PVDF (Mw. $5.34 \times 10^5$ g $mol^{-1}$) based simulated microplastic suspension (~0.001 g $mL^{-1}$).

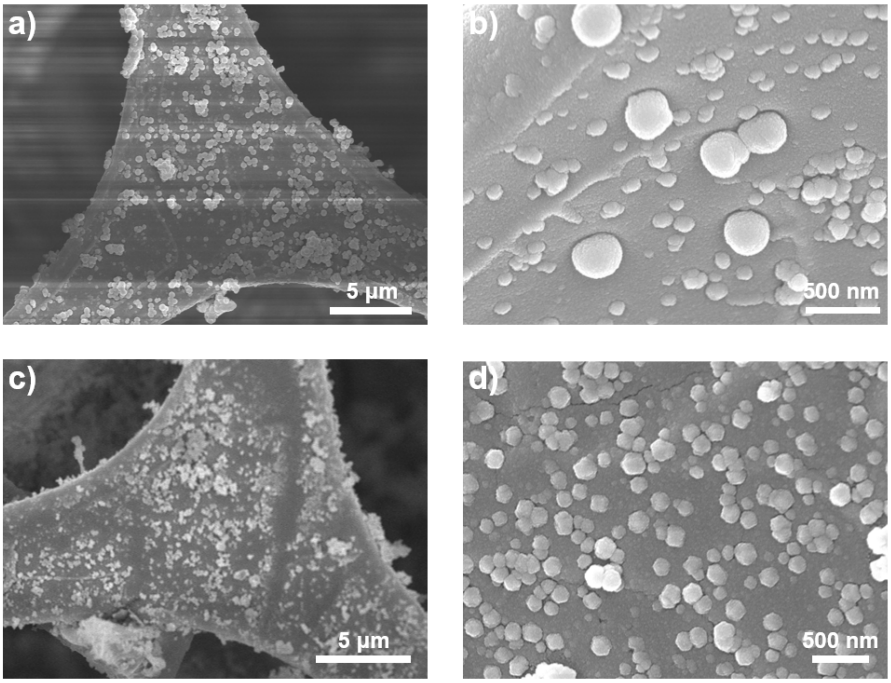


**Fig. S22** The SEM images of UiO-66-OH@MF-3 after microplastic removal test and recycled. a, b) UiO-66-OH@MF-3 after microplastic removal test. c, d) UiO-66-OH@MF-3 after filtration and washing with water for several times.

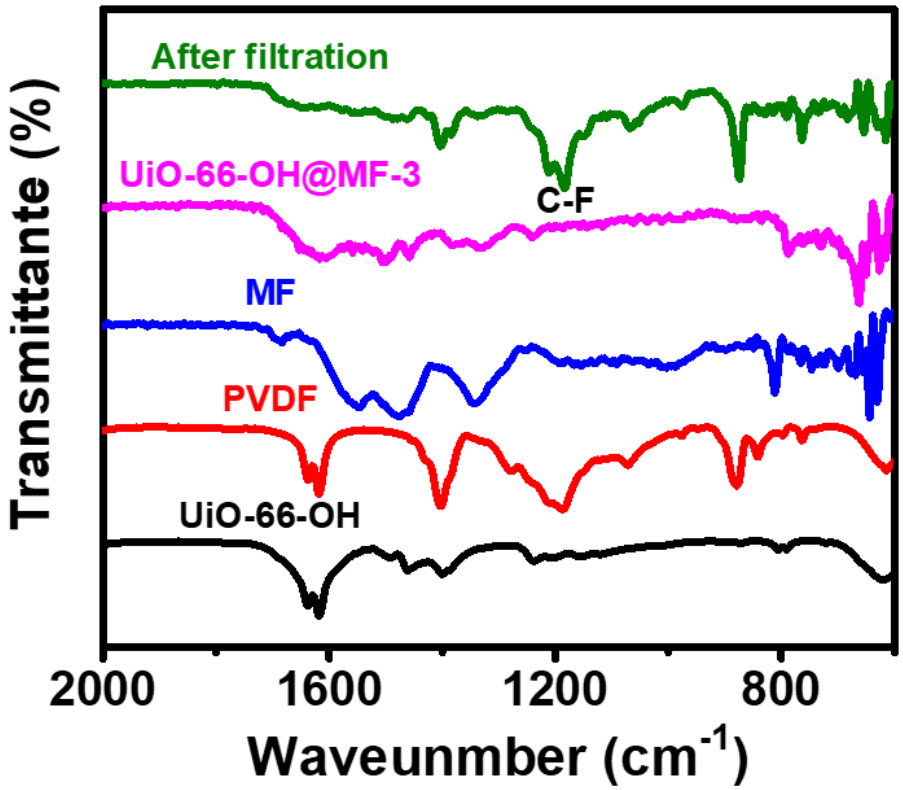


**Fig. S23** The FT-IR spectra of UiO-66-OH@MF before and after filtration, MF, PVDF and UiO-66-OH.

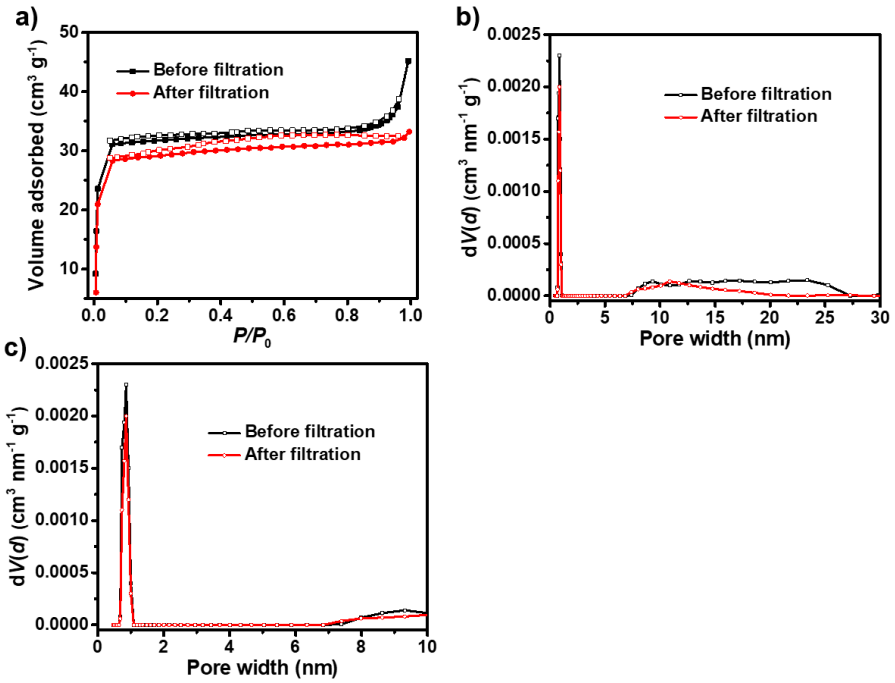


**Fig. S24** The $N_2$ sorption curves and pore size distribution of UiO-66-OH@MF-3 before and after filtration tests. a) The $N_2$ sorption curves. b) The pore size distribution (0-30 nm). c) The pore size distribution (0-10 nm). Before $N_2$ sorption tests, the UiO-66-OH@MF-3 after filtration test is washed with water for several times and dried at 150 $^{o}$C under vacuum for 24 h.

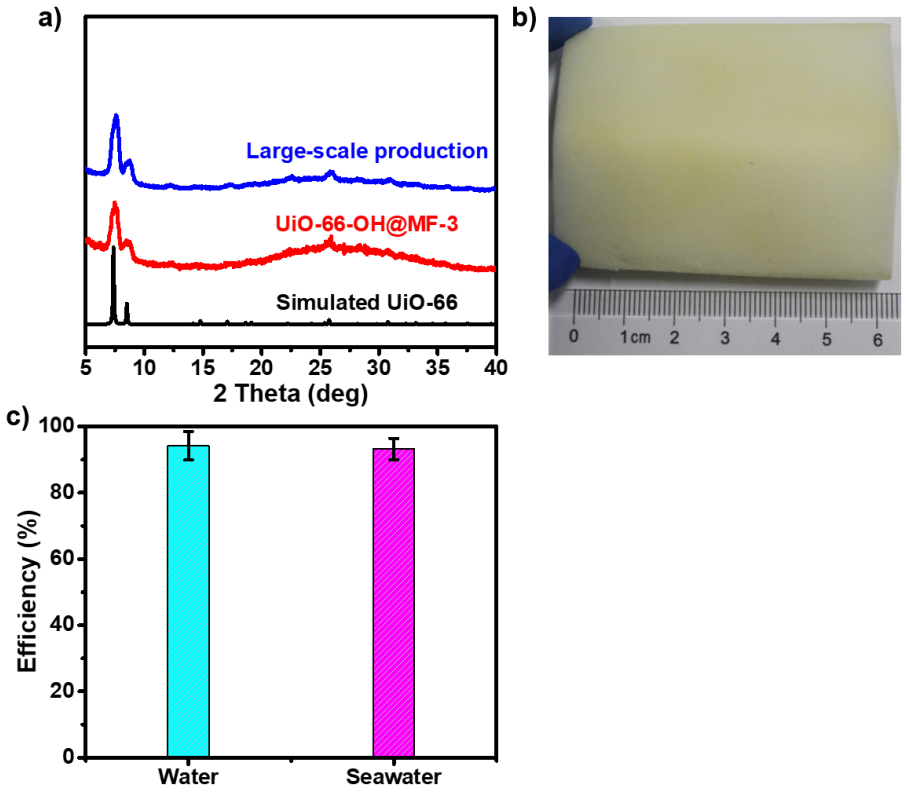


**Fig. S25** The characterization of UiO-66-OH@MF-3 obtained from scale-up production. a) The PXRD patterns. b) The photo image. c) The removal efficiency for PVDF (Mw. $5.34 \times 10^5$ g $mol^{-1}$) based simulated microplastic suspensions in both water and seawater.

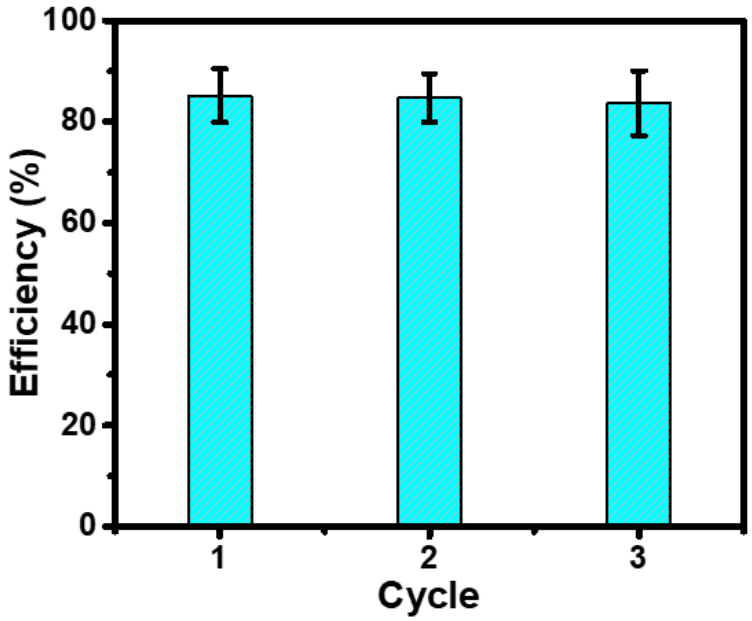


**Fig. S26** The recycle performances of UiO-66-OH@MF-3 in large-quantity tests.

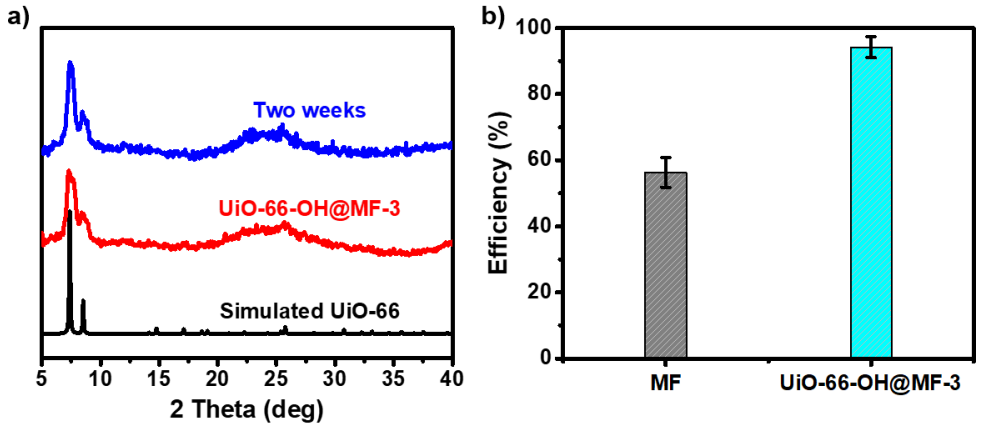


**Fig. S27** The stability and microplastic removal tests of UiO-66-OH@MF-3 in simulated seawater. a) The PXRD patterns of the stability test for UiO-66-OH@MF-3 in seawater. b) The removal efficiency of bare MF and UiO-66@MF-3.

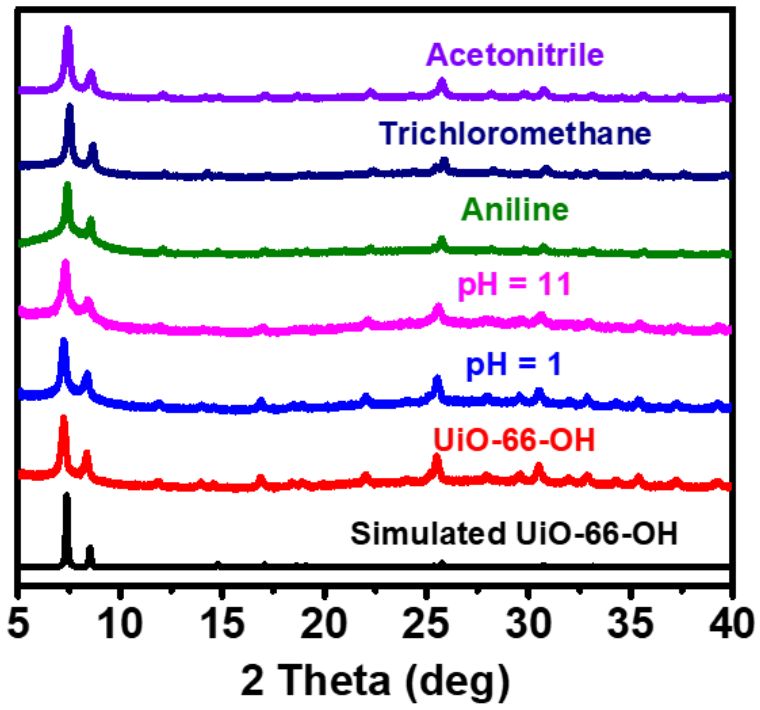


**Fig. S28** The PXRD patterns of the chemical stability tests for UiO-66-OH. During the tests, UiO-66-OH is immersed in relative solution for 24 h.

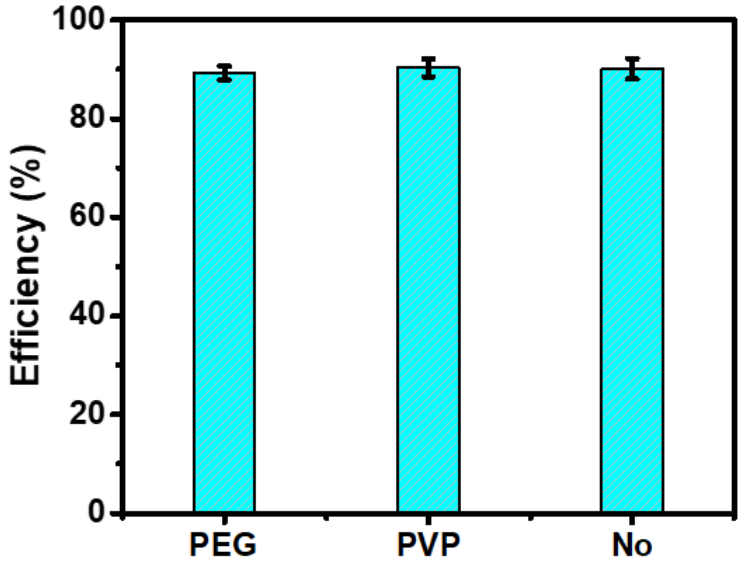


**Fig. S29** The efficiency of UiO-66-OH@MF-3 for the removal of PVDF suspension with the addition of different organic molecules.

a)

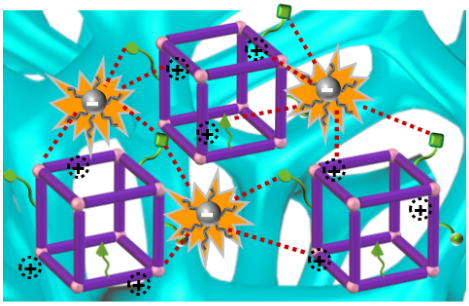

b)

| Advantages of foam materials | |
|---|---|
| Interpenetrated pore structure | Fast passage of solvent and sufficient contact |
| High stability | Long-term applications |
| Electrostatic interaction | High affinity to microplastics |
| Functional groups or metal sites | Possible interaction with microplastics |

**Fig. S30.** The possible interactions between microplastics and foam materials. a) The schematic presentation. b) The possible interactions and advantages of Zr-MOF based foam materials in microplastic removal. We have tried to apply the MOFs as microcrystalline powders or pellets for the removal of microplastics and tremendous efforts have been devoted. However, the dense microcrystalline powders will bring large pressure-drop in the filler and the integrity of MOF based pellets are hard be retained under the condition of flowing solvent. Besides, both of them would break down into tiny powders to affect the removal process. Based on advantages of Zr-MOF based foam materials, MOFs are more promising candidates than organic polymers owing to their lack of well-defined crystalline structure that can precisely control the surface charge, functional group or metal site as that of MOFs.

**Table S1** The $N_2$ sorption results of UiO-66-OH and UiO-66-OH@MF with different loadings.

| | Loading (wt%) | $S_{BET}$ ($m^2$ $g^{-1}$) | $V_t$ ($cm^3$ $g^{-1}$) |
|---|---|---|---|
| UiO-66-OH | - | 527 | 0.34 |
| UiO-66-OH@MF-2 | 13.0% | 62 | 0.022 |
| UiO-66-OH@MF-3 | 25.4% | 132 | 0.043 |